Extreme Mechanics Letters 83 (2026) 102455

Contents lists available at ScienceDirect

Extreme Mechanics Letters

journal homepage: www.elsevier.com/locate/eml

# Revealing surface tension in elastic membranes via indentation

Wanying Zheng [a,1], Zhida Gao [b,c,1], Chuanli Yu [a], Jun Yin [b,c,*], Zhaohe Dai [a,*]

[a] School of Mechanics and Engineering Science, State Key Laboratory for Turbulence and Complex Systems, Peking University, Beijing 100871, China
[b] State Key Laboratory of Mechanics and Control of Mechanical Structures, Key Laboratory for Intelligent Nano Materials and Devices of the Ministry of Education, Nanjing University of Aeronautics and Astronautics, Nanjing, 210016, China
[c] College of Aerospace Engineering, Nanjing University of Aeronautics and Astronautics, Nanjing, 210016, China

ARTICLE INFO

*Keywords:*
Indentation
Elastic membrane
Surface tension
Contact angle

ABSTRACT

When an elastic membrane is deformed, the external work is stored not only as volume-related elastic strain energy but also as area-related surface energies, since the total membrane area changes. The latter contribution is challenging to quantify experimentally, especially for ultrathin membranes. Here, we demonstrate that such surface effects can be revealed through indentation by comparing tests performed at gas and liquid interfaces. Specifically, using monolayer graphene indented across $N_2$–graphene and water–graphene interfaces, we show that graphene indented against water appears significantly softer—a signature of interfacial energetics favoring the water–graphene configuration. A membrane theory incorporating both elasticity and surface forces quantitatively reproduces the measured force–displacement curves, enabling the extraction of the interfacial tension difference and, in turn, membrane's wettability. These results establish indentation as a probe of solid–liquid surface tension at the membrane limit and highlight that surface effects – often regarded as negligible in 2D materials – must be carefully accounted for in applications ranging from straintronics to nanofluidics.

## 1. Introduction

When a membrane is subjected to external forces, the work is stored not only as elastic energy but also as surface energy associated with the increase in surface area [1,2]. In the simplest case of pure tension, a capillary membrane such as a soap film exhibits a constant force–displacement relation, while a purely elastic membrane follows Hookean behavior (Fig. 1A). When both elasticity and capillarity are present, the response is their superposition: the effective force–displacement curve is shifted such that the zero-force state corresponds to a slight negative strain (Fig. 1A). Consequently, direct measurement of surface tension in a membrane via simple tension is challenging because near the zero-force point, the elastocapillary response is indistinguishable from a purely elastic one. Only at relatively large tensions, where more complex surface stresses may emerge, might surface effects become apparent [3]. Alternatively, for a thin membrane with clamped edges subjected to transverse loading such as pressure, the Laplace law for a capillary membrane predicts a linear pressure–deflection relation at small deflections [4], whereas a purely elastic membrane exhibits a cubic dependence [5,6]. When both effects are present, their superposition produces a distinct elastocapillary response (Fig. 1B) [2].

At first glance, applying a transverse load seems to provide a straightforward route to measuring surface tension. In the field of 2D crystals, however, the situation is more subtle. Over the past two decades, indentation, blister, and bulge tests have been widely employed to probe their mechanics [7–16], yet the role of surface tension has remained elusive, as previous analyses have generally neglected it. A key reason is that pretension or residual tension in 2D crystals produces mechanical responses that closely mimic those of surface tension [2,6]. As a result, surface tension, pretension, and elastic stiffness enter the load–deflection response in a coupled manner, making their independent extraction from a single curve impossible.

In this work, we overcome this difficulty through indentation experiments in which the interfacial surface energy is tuned by varying the surrounding medium. Specifically, we perform atomic force microscopy (AFM) indentation tests on monolayer graphene, with the medium beneath the sheet controlled to be either nitrogen gas ($N_2$) or water. By contrasting the load–deflection curves measured at the $N_2$–graphene and water–graphene interfaces, we show that surface tension has a clear and measurable influence on the transverse response of 2D crystals. Moreover, we demonstrate that this contrast provides a route for determining the water contact angle of the 2D crystal—a quantity that has traditionally been difficult to measure.

* Corresponding authors.
*E-mail addresses:* yinjun@nuaa.edu.cn (J. Yin), daizh@pku.edu.cn (Z. Dai).
[1] These two authors contributed equally.

https://doi.org/10.1016/j.eml.2026.102455
Received 29 November 2025; Received in revised form 12 January 2026; Accepted 2 February 2026
Available online 4 February 2026

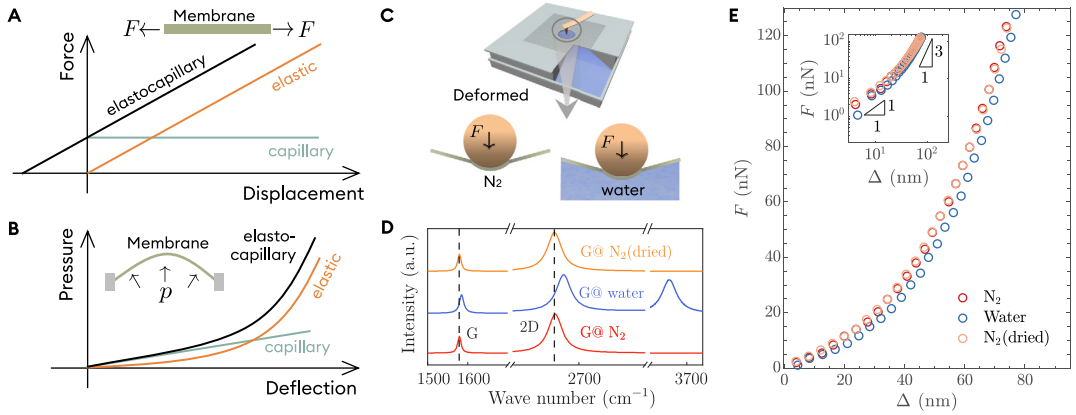


**Fig. 1.** Experimental framework for elastocapillarity. (A) Schematic load–displacement curves for capillary, elastic, and elastocapillary membranes under simple tension. (B) Schematic load–deflection curves for capillary, elastic, and elastocapillary membranes with clamped edges under transverse pressure. (C) Schematic of the AFM indentation setup. The surrounding medium, either $N_2$ or water, is controlled within the bottom chamber. We note that the dry membrane exhibits a slight initial sagging (depth < 4 nm), and that water injection slightly reduces this sagging depth. (D) Raman spectra of graphene interfacing with $N_2$, water, and $N_2$ after drying. All spectra are normalized to the intensity of the 2D peak. (E) Indentation force–displacement curves measured on the same graphene sample interfacing with $N_2$ (red markers) and water (blue markers). Yellow markers correspond to the same watered sample after drying. The inset shows the curves in logarithmic coordinates. (For interpretation of the references to color in this figure legend, the reader is referred to the web version of this article.)

## 2. Experiments

The indentation test is performed on a custom silicon nitride–silicon–silicon nitride (SiNx–Si–SiNx) substrate, illustrated in Fig. 1C (The substrate fabrication procedure is detailed in S1 of Supplementary material). A central channel is etched through the substrate, creating a direct path to the environmental chamber below. The chamber, made from 3D-printed stainless steel, is attached to the substrate and sealed with polydimethylsiloxane (PDMS) to form a closed medium delivery system (see details of the device in Fig. S2 of the Supplementary material). The upper SiNx layer of the substrate contains a circular opening with a radius of $\sim$ 1200 nm. During the indentation experiments, monolayer graphene, obtained by mechanical exfoliation, is transferred over this opening, creating the interfaces with the medium flowing through the channel.

Two types of graphene interfaces are examined in this work – $N_2$–graphene and water–graphene – achieved by switching the medium in the etched channel (see methods in S1 of the Supplementary material). Note that when water is introduced into the etched cavity, the device is positioned in a vacuum chamber and subjected to a vacuum of 80 kPa below ambient pressure for 10 min to eliminate any potential trapped air, thereby forming a well-contacted water–graphene interface. Raman spectroscopy is used to verify the interfacial condition (Fig. 1D). Relative to the $N_2$–graphene interface, the G and 2D peaks of the water–graphene interface are blue-shifted by 5.09 $cm^{-1}$ and 12.35 $cm^{-1}$, respectively, accompanied by an additional peak near 3400 $cm^{-1}$, consistent with strong water–graphene contact [17]. For a sample initially interfaced with $N_2$, then switched to water, and subsequently returned to $N_2$ (after solvent exchange and subsequent supercritical $CO_2$ drying), the Raman spectra of the $N_2$–graphene interface are fully restored after drying, confirming the reversibility of the process (Fig. 1D). This also rules out the possibility of complex swelling effects.

We first use tapping-mode AFM to screen for defects such as tears and wrinkles and to locate the suspended graphene region. Indentation tests are then performed at the center of the suspended area. Each sample is measured sequentially in three states: first with a $N_2$–graphene interface, then with the medium switched to water, and finally after drying back in a $N_2$ environment. During indentation, the AFM cantilever is first driven downward by a displacement $\Delta$, while the corresponding applied normal force $F$ is recorded. Once the preset maximum load of $\sim$ 140 nN is reached, the cantilever is retracted to release the force. The loading speed is fixed at 54 nm/s to ensure quasi-static conditions. For each medium, every sample is tested three times, and the resulting variability provides the error bars shown in Fig. 2D and 3B.

A representative set of force–displacement curves is shown in Fig. 1E. Both the $N_2$– and water–graphene interfaces follow the scaling law discussed in the Introduction [6,18]: as the indentation depth $\Delta$ increases, the response transitions from a pretension- or surface-tension–dominated linear regime to an elasticity-dominated cubic regime. This crossover occurs over a range of 20–60 nN. Importantly, for the same applied force, the water–graphene interface exhibits larger deflection than the $N_2$–graphene interface. This provides direct evidence that differences in surface energy influence the mechanical response of the membrane. The relatively softer response of the water–graphene interface further suggests that this configuration is energetically favored over the $N_2$–graphene interface. At larger indentation depths, however, the two curves become nearly parallel (inset of Fig. 1E), indicating that the intrinsic elasticity of the graphene sheet eventually dominates the response. We note that similar softening behavior was also reported by Ferrari et al. in [17], where it was attributed to differences in the initial geometry of graphene. In our case, however, the samples exhibit only a slight variation in the initial sagging depth (less than 5 nm), which is unlikely to account for the observed difference in mechanical response (see discussion of Fig. S3 in the Supplementary material).

## 3. Results and discussion

### 3.1. An elastocapillary model

We may interpret the results in Fig. 1E with reference to the schematic in Fig. 1B. For an elasticity-free membrane in the non-contact region, the resistance to transverse loading $p(r)$ is provided solely by the surface tension contributions from the top membrane-gas interface ($\gamma_{sg}$) and the bottom membrane-medium interface ($\gamma_{sm}$). In this case, the Young–Laplace equation gives

$$(\gamma_{sg} + \gamma_{sm})(\kappa_{rr} + \kappa_{\theta\theta}) + p = 0, \tag{1}$$

where $\kappa_{rr}$ and $\kappa_{\theta\theta}$ are the radial and hoop principal curvatures of the deformed surface. For a purely elastic membrane with a pretension $T$, the balance of forces is instead expressed as

$$N_{rr}\kappa_{rr} + N_{\theta\theta}\kappa_{\theta\theta} + p = 0, \tag{2}$$

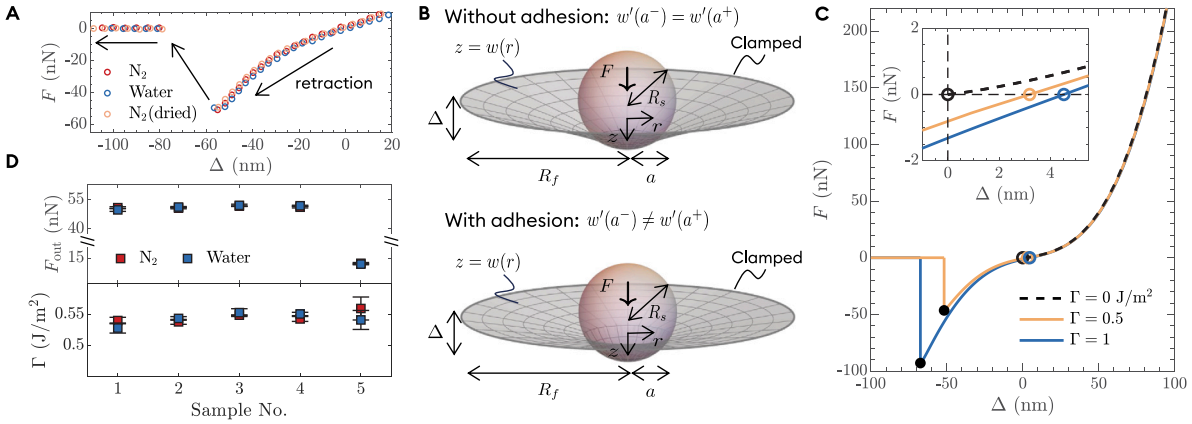


**Fig. 2.** Effects of interfacial adhesion on the mechanical response of elastic membranes. (A) Retracting force–displacement curves measured on the same graphene sample interfacing with $N_2$ (red markers) and water (blue markers). Yellow markers correspond to the same watered sample after drying. (B) Schematic illustration of contact between a thin membrane and a rigid indenter, with and without adhesion. The shape of the indenter is modeled as a sphere, according to the scanning electron microscope (SEM) imaging in Fig. S1 of the Supplementary material. (C) Numerically calculated force–displacement curves for different adhesion energies $\Gamma$, using $T = 0.1$ N/m, $R_s = 30$ nm, $R_f = 1200$ nm, and a typical graphene stiffness of 340 N/m. Hollow circles denote the zero-force (initial displacement) states, and filled black circles mark the pull-off force $F_{\text{out}}$. (D) Experimentally measured pull-off forces and the corresponding interface adhesion energies extracted for $N_2$– and water–graphene interfaces. (For interpretation of the references to color in this figure legend, the reader is referred to the web version of this article.)

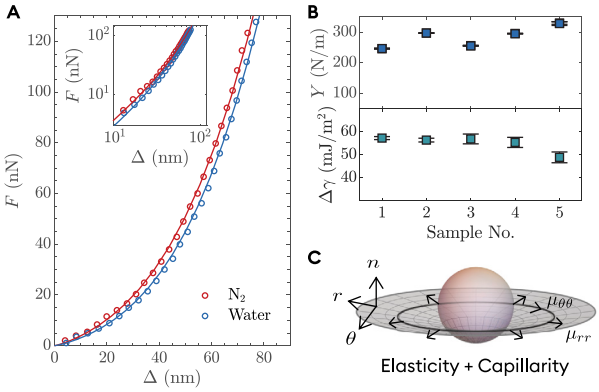


**Fig. 3.** Extracting surface tension difference by indentation. (A) Fitting of indentation force–displacement curves. The scatter points and solid lines represent the experimental data and numerical fitting curves, respectively. (B) Fitted in-plane stiffness of graphene and the corresponding differences in surface tension obtained from five sets of graphene samples. Note that the film radius for Sample No. 5 is ~1 μm and the radius of the indenter is ~7 nm. (C) Schematic of a deformed film subjected to general elastic and capillary forces.

where $N_{rr}$ and $N_{\theta\theta}$ are the radial and hoop stress resultants that need to be calculated according to the strain in the deformed membrane and Hooke's law [19]. When both effects are present, the membrane becomes elastocapillary. In this case, the governing equation naturally generalizes to

$$(N_{rr} + \gamma_{sg} + \gamma_{sm})\kappa_{rr} + (N_{\theta\theta} + \gamma_{sg} + \gamma_{sm})\kappa_{\theta\theta} + p = 0, \tag{3}$$

which is analogous to the equation for wetting problems on elastic membranes [2,20,21].

At small indentation depths, both the radial and hoop stresses in the membrane are governed by the pretension $T$ introduced during device fabrication, so that $N_{rr} = N_{\theta\theta} = T$. Using elementary geometry, $\kappa_{rr}, \kappa_{\theta\theta} \sim \Delta/R_f^2$, where $R_f$ is the radius of the suspended membrane [18], the governing Eq. (3) yields

$$F \propto (T + \gamma_{sg} + \gamma_{sm})\,\Delta, \tag{4}$$

indicating that the initial linear force–displacement response is controlled by the combined contribution of pretension and surface tensions. A more detailed analysis shows that the prefactor includes a weak logarithmic correction [22]. At larger indentation depths, the membrane experiences significant stretching, with the stress resultants scaling with the stretching stiffness $Y$ and the strain $\sim (\Delta/R_f)^2$ [6,18]. This leads to the classical cubic scaling law

$$F \propto \frac{Y}{R_f^2}\,\Delta^3, \tag{5}$$

which is independent of surface energy. Consequently, the overall response transitions smoothly from a quasi-linear regime controlled by $(T + \gamma_{sg} + \gamma_{sm})$ at small $\Delta$ to a cubic regime governed solely by the intrinsic elastic stiffness $Y$ at large $\Delta$, in excellent agreement with the experimentally observed force–displacement curves in Fig. 1E.

### 3.2. Effect of adhesion

It is natural to exploit the linear regime of the mechanical response to quantify the difference in $\gamma_{sm}$ between the $N_2$– and water–graphene interfaces. However, this analysis is complicated by possible adhesion between the indenter and the membrane: adhesive contact can shift the apparent zero-force point, introducing a finite deflection even in the absence of load due to the interplay between adhesion and elasticity [23]. This effect can also manifest during the retraction process, where a finite pull-off force is required to fully separate the indenter from the membrane, as shown in Fig. 2A. To clarify the role of adhesion, we apply a model based on total free-energy minimization that incorporates both surface tension and adhesion, following the approaches of [24–26]. The theoretical details are presented in S2 of the Supplementary material.

A particularly notable feature of adhesion is the emergence of a kink at the contact line ($r = a$ in Fig. 2B). In the absence of adhesion, the membrane profile is smooth, yielding Hertz-like contact behavior in which zero force corresponds to zero displacement (dashed curve in Fig. 2C). By contrast, the kink induced by adhesion introduces a small initial deflection even at zero force (colored curves in Fig. 2C), reflecting the coupling between adhesion and elasticity. This apparent pre-deflection makes the membrane seem artificially stiffer in the initial regime when adhesion energy is large, thereby complicating the extraction of surface tension.

Fortunately, in our experiments, the adhesion effect is relatively weak, owing to the small indenter size (the radius of the indenter for the first four samples, $R_s \approx 30$ nm, and for Sample No. 5, $R_s \approx 7$ nm) and the moderate adhesion energy. The adhesion energy $\Gamma$ between the

sphere and the membrane can be directly estimated from the measured pull-off force $F_{out}$ using

$$\Gamma = F_{out}/(\pi R_s). \tag{6}$$

Remarkably, this relation is independent of membrane size, surface tension, and even the constitutive law of the material [26]. Using this expression, we obtain $\Gamma$ values on the order of 0.5 J/m$^2$ for graphene interfaced with both $N_2$ and water (Fig. 2D). This indicates that the underlying medium does not significantly influence adhesion, consistent with recent measurements showing the transparency of graphene to van der Waals forces [25]. In Fig. 2C, we plot numerically calculated force–displacement curves for our experimental system under varying levels of adhesion and zero surface tension (i.e., $\gamma_{sg} + \gamma_{sm} = 0$). For experimental parameters ($R_s \approx 30$ nm, $R_f \approx 1200$ nm for Samples No. 1–4, and $R_s \approx 7$ nm, $R_f \approx 1000$ nm for Sample No. 5), the curves with and without adhesion show negligible differences. This indicates that the variation in the initial stiffness observed in Fig. 1E should arise from differences in surface tension rather than adhesion. We note that for larger indenters, however, adhesion effects become significant and would result in a substantial contact area. In such cases, the change in the medium within this contact region must be carefully considered, introducing a good deal of complexity that could hinder a clear interpretation of the surface tension.

### 3.3. Comparison with experiments

We then apply the elastocapillary model in Eq. (3) to interpret the indentation results for graphene interfacing with $N_2$ and water. Since an analytical solution to Eq. (3) is not feasible due to intrinsic geometric nonlinearities [6,18], we solve the problem numerically. The model involves only two fitting parameters: the combined pretension and surface contributions, $\gamma = T + \gamma_{sg} + \gamma_{sm}$ (which governs the small-depth response), and the in-plane stiffness $Y$ of graphene (which dominates the large-depth response). These parameters are adjusted to reproduce the experimental force–displacement curves (Fig. 3A), while adhesion effects are neglected (see justification in Fig. S4 of the Supplementary material).

Importantly, for each sample with the interfacing medium switched from $N_2$ to water, $Y$ remains physically unchanged, while only $\gamma$ is allowed to vary to account for the difference in mechanical response. We find $Y$ consistently in the range of 250–330 N/m across all samples (Fig. 3B), while $\gamma$ ranges from $\sim$ 100.5 mJ/m$^2$ to $\sim$ 243.5 mJ/m$^2$. Although the absolute value of $\gamma$ is not itself meaningful, the relative change in $\gamma$ between the two interfaces directly gives the surface energy difference

$$\Delta\gamma = \gamma_{sg} - \gamma_{sl}, \tag{7}$$

where $\gamma_{sg}$ and $\gamma_{sl}$ are the surface energies of the gas–graphene and liquid–graphene interfaces, respectively. From our measurements, we find a significant reduction in surface tension, with $\Delta\gamma$ in the range of 48.9 $\sim$ 57.3 mJ/m$^2$ (Fig. 3B).

It is worth noting that the surface energy of a membrane, in principle, depends on the in-plane strain state $\epsilon$ through the Shuttleworth effect [27]. Accordingly, a more general form of the elastocapillary Eq. (3) in axisymmetry can be written as $\mu_{rr}\kappa_{rr} + \mu_{\theta\theta}\kappa_{\theta\theta} + p = 0$, where $\mu_{rr} = N_{rr} + \gamma_{sg}(\epsilon) + \gamma_{sm}(\epsilon)$ and $\mu_{\theta\theta} = N_{\theta\theta} + \gamma_{sg}(\epsilon) + \gamma_{sm}(\epsilon)$ are the effective stress resultants, and $\gamma_{sg}(\epsilon)$ and $\gamma_{sm}(\epsilon)$ denote the strain-dependent surface stresses [20,28–31]. This formulation highlights that the elastocapillary response can, in general, be considerably more complex than a simple superposition of constant surface energies, as illustrated in Fig. 3C. In the present work, however, we restrict our attention to moderate deflections corresponding to small in-plane strains (typically below 1%), well within the range where Shuttleworth effects are negligible. Nonetheless, extending such studies to more deformable membranes such as elastomer films would provide an opportunity to probe strain-dependent surface stresses at larger strains.

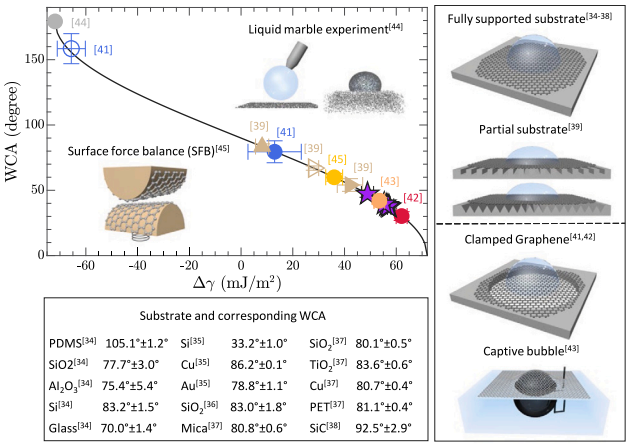


**Fig. 4.** Surface energy differences and contact angles measured by various methods. For literature in which WCA is known, the interfacial energy difference is calculated according to Eq. (8).

### 3.4. Implications for wettability

Lastly, we extend the discussion of $\Delta\gamma$ to wettability, which has been reported very inconsistently in the literature, with water contact angles (WCA), $\theta_c$, ranging from about 30° to nearly 180° [32–45]. Our indentation tests of graphene with wet and dry interfaces provide a different way to estimate this property. In particular, using Young's relation [46], the water contact angle on graphene can be calculated from the surface energy difference as

$$\cos\theta_c = \Delta\gamma/\gamma_{lg}, \tag{8}$$

where $\gamma_{lg}$ is the liquid–gas interfacial energy. Using the values in Fig. 3B, we find that the WCA ranges from 37.3° to 47.2°, indicating that graphene is hydrophilic.

In Fig. 4, we summarize representative approaches reported in the literature for measuring the WCA of graphene. These methods include: (i) direct WCA measurements on substrate-supported graphene [34–39]; (ii) measurements on suspended graphene, such as clamped free-standing films [41,42] or through captive-bubble techniques [43]; and (iii) indirect assessments of wettability, for example, via adsorption experiments (e.g., the liquid marble method [44]) or surface energy measurements (e.g., surface force balance [45]). Method (i) is complicated by substrate effects, as variations in substrate material and geometry can lead to significant scatter in the reported WCAs of graphene. By contrast, our results are consistent with those of Refs. [42,43], where measurements were performed directly on suspended graphene (Fig. 4). This agreement suggests that probing the out-of-plane mechanical response of an elastic sheet offers a promising route for surface energy metrology, which is typically challenging for ultrathin membranes.

## 4. Conclusions

In summary, we have demonstrated that the surface tension of monolayer graphene can be directly probed via nanoindentation by contrasting its mechanical response at gas and liquid interfaces. Our experiments reveal that the water–graphene interface is mechanically softer than the $N_2$–graphene interface, providing a clear signature of interfacial energy effects. By combining indentation measurements with a minimal elastocapillary model, we extract the surface energy difference and deduce the water contact angle of graphene, highlighting its hydrophilic nature at the atomic limit though disentangling surface tension from pretension remains difficult. Beyond fundamental insights into the mechanics of 2D crystals, this approach establishes indentation as a versatile tool for quantifying surface forces in ultrathin materials,

offering opportunities to explore strain-dependent surface stresses, wettability tuning, and interfacial phenomena in more complex membranes and heterostructures in the future.

## CRediT authorship contribution statement

**Wanying Zheng:** Writing – original draft, Methodology, Investigation, Formal analysis. **Zhida Gao:** Writing – original draft, Investigation, Formal analysis. **Chuanli Yu:** Methodology, Investigation. **Jun Yin:** Writing – review & editing, Methodology, Investigation. **Zhaohe Dai:** Writing – review & editing, Investigation, Conceptualization.

## Declaration of competing interest

The authors declare that they have no known competing financial interests or personal relationships that could have appeared to influence the work reported in this paper.

## Acknowledgment

This work was supported by the National Natural Science Foundation of China (Grant Nos. 12372103 and 12432003).

## Appendix A. Supplementary data

Supplementary material related to this article can be found online at https://doi.org/10.1016/j.eml.2026.102455.

## Data availability

Data will be made available on request.

## References

[1] J. Bico, É. Reyssat, B. Roman, Elastocapillarity: When surface tension deforms elastic solids, Annu. Rev. Fluid Mech. 50 (2018) 629–659.
[2] D. Vella, M. Adda-Bedia, E. Cerda, Capillary wrinkling of elastic membranes, Soft Matter 6 (22) (2010) 5778–5782.
[3] B. Andreotti, J.H. Snoeijer, Statics and dynamics of soft wetting, Annu. Rev. Fluid Mech. 52 (1) (2020) 285–308.
[4] P.-G. De Gennes, F. Brochard-Wyart, D. Quéré, Capillarity and Wetting Phenomena: Drops, Bubbles, Pearls, Waves, Springer Science & Business Media, 2003.
[5] Z. Dai, Y. Rao, N. Lu, Two-dimensional crystals on adhesive substrates subjected to uniform transverse pressure, Int. J. Solids Struct. 257 (2022) 111829.
[6] D. Vella, B. Davidovitch, Indentation metrology of clamped, ultra-thin elastic sheets, Soft Matter 13 (2017) 2264–2278.
[7] C. Lee, X. Wei, J.W. Kysar, J. Hone, Measurement of the elastic properties and intrinsic strength of monolayer graphene, Science 321 (2008) 385–388.
[8] S.P. Koenig, N.G. Boddeti, M.L. Dunn, J.S. Bunch, Ultrastrong adhesion of graphene membranes, Nat. Nanotechnol. 6 (9) (2011) 543–546.
[9] S. Bertolazzi, J. Brivio, A. Kis, Stretching and breaking of ultrathin MoS2, ACS Nano 5 (12) (2011) 9703–9709.
[10] N.G. Boddeti, S.P. Koenig, R. Long, J. Xiao, J.S. Bunch, M.L. Dunn, Mechanics of adhered, pressurized graphene blisters, J. Appl. Mech. 80 (4) (2013) 040909.
[11] Z. Cao, P. Wang, W. Gao, L. Tao, J. Suk, R. Ruoff, D. Akinwande, R. Huang, K. Liechti, A blister test for interfacial adhesion of large-scale transferred graphene, Carbon 69 (2014) 390–400.
[12] D. Lloyd, X. Liu, N. Boddeti, L. Cantley, R. Long, M.L. Dunn, J.S. Bunch, Adhesion, stiffness, and instability in atomically thin MoS2 bubbles, Nano Lett. 17 (9) (2017) 5329–5334.
[13] Z. Dai, Y. Hou, D.A. Sanchez, G. Wang, C.J. Brennan, Z. Zhang, L. Liu, N. Lu, Interface-governed deformation of nanobubbles and nanotents formed by two-dimensional materials, Phys. Rev. Lett. 121 (26) (2018) 266101.
[14] G. Wang, Z. Dai, J. Xiao, S. Feng, C. Weng, L. Liu, Z. Xu, R. Huang, Z. Zhang, Bending of multilayer van der Waals materials, Phys. Rev. Lett. 123 (11) (2019) 116101.
[15] Z. Fang, Z. Dai, B. Wang, Z. Tian, C. Yu, Q. Chen, X. Wei, Pull-to-peel of two-dimensional materials for the simultaneous determination of elasticity and adhesion, Nano Lett. 23 (2) (2022) 742–749.
[16] M. Calis, D. Lloyd, N. Boddeti, J.S. Bunch, Adhesion of 2D MoS2 to graphite and metal substrates measured by a blister test, Nano Lett. 23 (7) (2023) 2607–2614.
[17] G.A. Ferrari, A.B. de Oliveira, I. Silvestre, M.J.S. Matos, R.J.C. Batista, T.F.D. Fernandes, L.M. Meireles, G.S.N. Eliel, H. Chacham, B.R.A. Neves, R.G. Lacerda, Apparent softening of wet graphene membranes on a microfluidic platform, ACS Nano 12 (2018) 4312–4320.
[18] Z. Dai, N. Lu, Poking and bulging of suspended thin sheets: Slippage, instabilities, and metrology, J. Mech. Phys. Solids 149 (2021) 104320.
[19] E.H. Mansfield, The Bending and Stretching of Plates, second ed., Cambridge University Press, 1989.
[20] Y. Liu, Y. Wei, Effect of surface energy on the indentation response of hard nanofilm/soft substrate composite structure, Int. J. Mech. Sci. 185 (2020) 105759.
[21] Y. Rao, S. Qiao, Z. Dai, N. Lu, Elastic wetting: Substrate-supported droplets confined by soft elastic membranes, J. Mech. Phys. Solids 151 (2021) 104399.
[22] T.G. Chandler, D. Vella, Indentation of suspended two-dimensional solids: The signatures of geometrical and material nonlinearity, J. Mech. Phys. Solids 144 (2020) 104109.
[23] M. Ciavarella, J. Joe, A. Papangelo, J. Barber, The role of adhesion in contact mechanics, J. R. Soc. Interface 16 (151) (2019) 20180738.
[24] F.M. Borodich, B.A. Galanov, Contact probing of stretched membranes and adhesive interactions: graphene and other two-dimensional materials, Proc. R. Soc. A 472 (2016) 20160550.
[25] C. Yu, W. Zeng, Z. Kou, W. Wang, L. Wang, Q. Li, X. Liu, Z. Dai, Transparency of graphene to solid-solid van der Waals interactions, Phys. Rev. Lett. 135 (15) (2025) 156202.
[26] W. Zheng, Z. Dai, Universal pull-off force for separating a rigid sphere from a membrane, J. Mech. Phys. Solids 201 (2025) 106163.
[27] R. Shuttleworth, The surface tension of solids, Proc. Phys. Soc. A 63 (1950) 444.
[28] M. Gurtin, A. Murdoch, Surface stress in solids, Int. J. Solids Struct. 14 (1978) 431–440.
[29] H.L. Duan, J. Wang, B.L. Karihaloo, Theory of elasticity at the nanoscale, Adv. Appl. Mech. 42 (2009) 1–68.
[30] R.W. Style, A. Jagota, C.-Y. Hui, E.R. Dufresne, Elastocapillarity: Surface tension and the mechanics of soft solids, Annu. Rev. Condens. Matter Phys. 8 (2017) 99–118.
[31] Q. Xu, K.E. Jensen, R. Boltyanskiy, R. Sarfati, R.W. Style, E.R. Dufresne, Direct measurement of strain-dependent solid surface stress, Nat. Commun. 8 (2017) 555.
[32] P. Snapp, J.M. Kim, C. Cho, J. Leem, M.F. Haque, S. Nam, Interaction of 2D materials with liquids: wettability, electrochemical properties, friction, and emerging directions, NPG Asia Mater. 12 (1) (2020) 22.
[33] C. Yu, Z. Dai, Characterizing the wetting behavior of 2D materials: a review, J. Mater. Informatics 3 (3) (2023) N–A.
[34] F. Du, J. Huang, H. Duan, C. Xiong, J. Wang, Wetting transparency of supported graphene is regulated by polarities of liquids and substrates, Appl. Surf. Sci. 454 (2018) 249–255.
[35] J. Rafiee, X. Mi, H. Gullapalli, A.V. Thomas, F. Yavari, Y. Shi, P.M. Ajayan, N.A. Koratkar, Wetting transparency of graphene, Nat. Mater. 11 (2012) 217–222.
[36] Y. Zhao, G. Wang, W. Huang, X. Fan, Y. Deng, J. Zhang, T. Wei, R. Duan, J. Wang, L. Sun, Investigations on the wettability of graphene on a micron-scale hole array substrate, RSC Adv. 6 (2016) 1999–2003.
[37] X. Li, Z. Li, Y. Long, Y. He, B. Li, J. Li, H. Qiu, J. Yin, W. Guo, Wetting stability of supported graphene in ambient environment, Adv. Eng. Mater. 24 (2022) 2101283.
[38] Y.J. Shin, Y. Wang, H. Huang, G. Kalon, A.T.S. Wee, Z. Shen, C.S. Bhatia, H. Yang, Surface-energy engineering of graphene, Langmuir 26 (2010) 3798–3802.
[39] T. Ondarçuhu, V. Thomas, M. Nuñez, E. Dujardin, A. Rahman, C.T. Black, A. Checco, Wettability of partially suspended graphene, Sci. Rep. 6 (2016) 24237.
[40] E. Kim, D. Kim, K. Kwak, Y. Nagata, M. Bonn, M. Cho, Wettability of graphene, water contact angle, and interfacial water structure, Chem 8 (2022) 1187–1200.
[41] H. Wang, D. Orejon, D. Song, X. Zhang, G. McHale, H. Takamatsu, Y. Takata, K. Sefiane, Non-wetting of condensation-induced droplets on smooth monolayer suspended graphene with contact angle approaching 180 degrees, Commun. Mater. 3 (2022) 75.
[42] J. Zhang, K. Jia, Y. Huang, X. Liu, Q. Xu, W. Wang, R. Zhang, B. Liu, L. Zheng, H. Chen, P. Gao, S. Meng, L. Lin, H. Peng, Z. Liu, Intrinsic wettability in pristine graphene, Adv. Mater. 34 (2022) 2103620.
[43] A.V. Prydatko, L.A. Belyaeva, L. Jiang, L.M.C. Lima, G.F. Schneider, Contact angle measurement of free-standing square-millimeter single-layer graphene, Nat. Commun. 9 (2018) 4185.
[44] B. Bera, N. Shahidzadeh, H. Mishra, L.A. Belyaeva, G.F. Schneider, D. Bonn, Wetting of water on graphene nanopowders of different thicknesses, Appl. Phys. Lett. 112 (2018) 151606.
[45] C.D. van Engers, N.E.A. Cousens, V. Babenko, J. Britton, B. Zappone, N. Grobert, S. Perkin, Direct measurement of the surface energy of graphene, Nano Lett. 17 (2017) 3815–3821.
[46] T. Young, An essay on the cohesion of fluids, Abstr. Pap. Philos. Trans. R. Soc. Lond. 1 (1997) 171–172.